GDCh

Research Articles

Angewandte
Chemie
International Edition
www.angewandte.org

Organocatalysis

Chiral Phosphoric Acid Catalyzed Conversion of Epoxides into Thiiranes: Mechanism, Stereochemical Model, and New Catalyst Design

Meng Duan+, Christian David Díaz-Oviedo+, Yang Zhou, Xiangyang Chen, Peiyuan Yu, Benjamin List,* Kendall N. Houk,* and Yu Lan*

Abstract: Computations and experiments leading to new chiral phosphoric acids (CPAs) for epoxide thionations are reported. Density functional theory calculations reveal the mechanism and origin of the enantioselectivity of such CPA-catalyzed epoxide thionations. The calculated mechanistic information was used to design new efficient CPAs that were tested experimentally and found to be highly effective. Bulky ortho-substituents on the 3,3′-aryl groups of the CPA are important to restrict the position of the epoxide in the key transition states for the enantioselectivity-determining step. Larger para-substituents significantly improve the enantioselectivity of the reaction.

Introduction

Chiral phosphoric acids are arguably the best known class of acidic organocatalysts in the literature,[1] with many reports on their efficient activity as catalysts for a wide range of organic transformations with potential applications in both industry and academia.[2] The success of this privileged motif relies in part on its bifunctional character, where the hydroxy group is a Brønsted acid,[3] while the phosphoryl oxygen atom acts as a Brønsted base.[4] This balance of Brønsted acidity/basicity as well as the steric demands of the catalyst can be finely tuned by careful choice of the substituents attached to the phosphoric acid moiety.[5,6] Chiral phosphoric acid (CPA) catalysis has become an important field in enantioselective synthesis.[7]

Among the several chiral backbones available in the literature, 1,1′-bi-2-naphthol (BINOL) stands out, as Brønsted acids derived therefrom have become a prominent group of catalysts, with high catalytic activity under mild reaction conditions.[8] The binaphthyloxyl group can be further functionalized by attaching substituents, which provides a variety of catalysts for enantioselective synthesis.[9] Small changes to the properties (steric and/or electronic) of these substituents can lead to significant differences in the observed enantioselectivities.[10] The development of a particular transformation in a highly enantioselective fashion generally involves the preparation and testing of a large number of CPAs.[11] Increasingly, theoretical calculations have proven to be a useful tool to design and computationally screen CPAs, and this approach can potentially reduce the experimental workload.[12]

The efficiency and robustness of chiral CPAs can also be applied to the kinetic resolution of racemic reactants.[13] Recently, the List group reported a highly efficient method for the synthesis of thiiranes by epoxide thionation through kinetic resolution using CPA (*R*)-**C1** as the catalyst and thiolactam **3a** as the sulfur donor (Scheme 1).[14] Considering the importance of enantiopure epoxides as building blocks in chemical synthesis, we were motivated to further understand this underdeveloped transformation. To clarify the mechanism and chirality transfer process of this reaction, we resorted to density functional theory (DFT) calculations. Ultimately, these calculations led to several designed CPAs that were predicted to perform the target kinetic resolution in a highly selective fashion. These predictions were confirmed experimentally.

Computational Methods. Geometry optimizations and frequency calculations were performed using the B3LYP functional with the 6-31G(d) basis set.[4a,7a,15] Normal vibrational mode analysis was carried out for all stationary points to confirm them as local minima or saddle points, and to derive the thermochemical corrections for the enthalpies and free energies. Single-point energies and solvent effects in chloroform were computed with the SMD solvation

[*]   Dr. M. Duan,+ Prof. Dr. Y. Lan
Green Catalysis Center, and College of Chemistry
Zhengzhou University, Zhengzhou, Henan 450001 (China)
E-mail: lanyu@cqu.edu.cn

Dr. M. Duan,+ Dr. X. Chen, Prof. Dr. K. N. Houk
Department of Chemistry and Biochemistry
University of California, Los Angeles, CA 90095 (USA)
E-mail: houk@chem.ucla.edu

C. D. Díaz-Oviedo,+ Prof. Dr. B. List
Max-Planck-Institut für Kohlenforschung
45470 Mülheim an der Ruhr (Germany)
E-mail: list@mpi-muelheim.mpg.de

Dr. M. Duan,+ Y. Zhou, Prof. Dr. P. Yu
Department of Chemistry and Shenzhen Grubbs Institute
Guangdong Provincial Key Laboratory of Catalysis
Southern University of Science and Technology
Shenzhen, 518055 (China)

[+]   These authors contributed equally to this work.
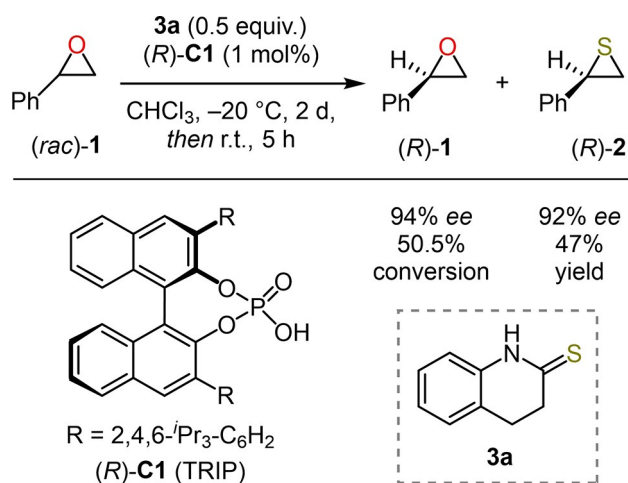
Scheme 1. CPA-catalyzed epoxide thionation with thiolactam **3a** by kinetic resolution.

model at the M06-2X/6-311+G(d,p) level of theory using the gas-phase-optimized structures.[16] A variety of other functionals were tested to verify the calculated selectivities. All calculations were performed using Gaussian 09.[17]

Results and Discussion

Computational Investigations. Previous experimental observations led to the proposed general catalytic cycle for the CPA-catalyzed epoxide thionation shown in Figure 1. CPA (*R*)-**C1** interacts with thiolactam **3a** to give heterodimer **I**; this association process is slightly endergonic by 0.2 kcal mol⁻¹. Complex **I** reacts with the epoxide by intermolecular nucleophilic substitution reaction via transition state **TS1**, which is activated by the hydrogen bond with the phosphoric acid. The reaction is a backside S$_N$2 process, but at the substituted carbon atom of the epoxide, partially resembling an S$_N$1 process. Ring-opened iminothioate intermediate **II** irreversibly forms, but can reversibly form the isomer **IV** via cyclic intermediate **III**. This isomerization proceeds by intramolecular nucleophilic addition of the hydroxy group to the imido moiety, which occurs via transition state **TS2** to give oxathiaazaspirodecane species **III**. Proton transfer from the CPA to the imido moiety induces an intramolecular S$_N$2 substitution to yield thiirane product **2**. The regenerated catalyst associates with another molecule of thiolactam **3a**, releasing the corresponding side-product lactam **4b**.

DFT calculations revealed that the enantioselectivity-determining step of this kinetic resolution is the CPA-assisted nucleophilic ring-opening of the epoxide by the thiolactam via the transition states **TS1-*R*** or **TS1-*S***. The calculated relative free energy of ring-open transition state **TS1-*S*** with *R*-epoxide **1** is 1.9 kcal mol⁻¹ higher than that of

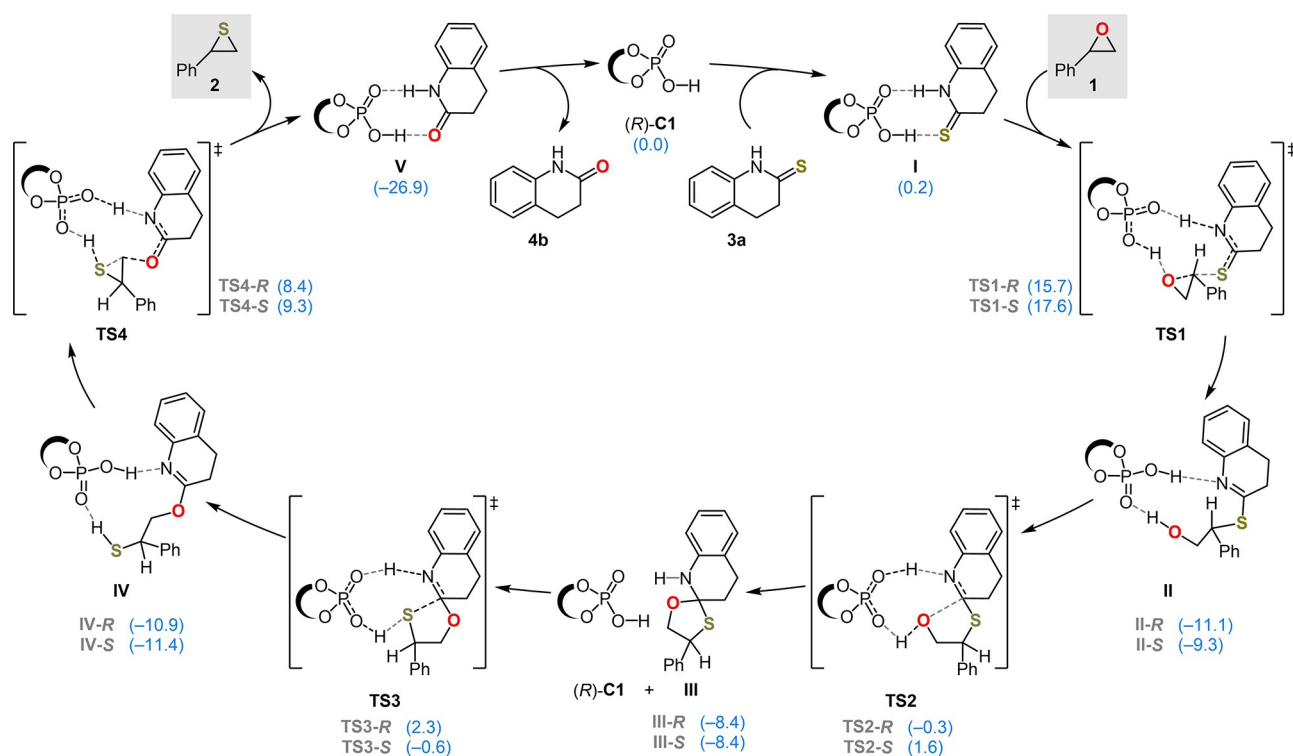**Figure 1.** Proposed catalytic cycle for the CPA-catalyzed epoxide thionation. The DFT-calculated free energies, in kcal mol⁻¹, are shown in parentheses. The stereochemical indicators *R*/*S* for all intermediates and transition states refer to the enantiomer of the thiirane obtained for each pathway.

transition state **TS1-R** with the *S*-epoxide. Based on this energy difference, the calculated *ee* value is 92%, in agreement with the experimental observation (92% *ee*).

The distortion (ΔE_{dist}) and interaction (ΔE_{int}) energies of the key transition states **TS1-R** and **TS1-S** were calculated to analyze the origin of the stereoselectivity of the reaction (Table S1).[18] In this analysis, transition states **TS1-R** and **TS1-S** were divided into three parts: catalyst, epoxide, and thiolactam. The calculated E_{dist} values of the catalyst and epoxide components in **TS1-S** are 5.9 and 1.0 kcal mol^{-1} higher than those in **TS1-R** (57.9 and 24.6 kcal mol^{-1}), respectively. The E_{dist} value of the thiolactam segment in **TS1-R** (1.0 kcal mol^{-1}) is almost the same as that in **TS1-S** (1.2 kcal mol^{-1}). The calculated difference in E_{int} between **TS1-R** (-102.2 kcal mol^{-1}) and **TS1-S** (-107.2 kcal mol^{-1}) is 5.0 kcal mol^{-1}. These results suggest that the difference in the reactivity of the two epoxide enantiomers is a consequence of the larger ΔE_{dist} value of the catalyst in **TS1-S**.

The origins of the different distortion energies for transition states **TS1-R** and **TS1-S** can be visualized from the corresponding calculated geometries (Figure 2). In **TS1-S**, the phenyl group from the reacting epoxide group is oriented toward the bulky isopropyl substituent of the catalyst (Figure 2(a,c)). Therefore, the dihedral angle C1-C2-C3-H1 of the CPA catalyst moiety in **TS1-S** rotates to $-8.5°$, which is significantly different from the original position (almost 0°), and suggests that the catalyst changes to an unfavorable conformation due to steric repulsion with the phenyl group of the reacting epoxide.

To better demonstrate this twisting of the catalyst structure, the axial projections of (*R*)-**C1**, **TS1-R**, and **TS1-S** are overlaid in Figure 2(b). This shows that the catalyst moiety in **TS1-S** is distorted from the original position, leading to a visible difference between the **TS1-S** (red) and (*R*)-**C1** (black) structures. Moreover, the unfavorable transition state **TS1-S** is also shifted further along the reaction coordinate, as reflected by the forming C–S bond being shorter. This causes a relatively large interaction with a larger unstable distortion in **TS1-S** than that in **TS1-R**. Therefore, distortion of the catalyst is responsible for the observed enantioselectivities.

These theoretical calculations indicate that the isopropyl group plays a key role in the determination of the enantioselectivity in the first S$_N$2-type ring opening of the epoxide (Figure 3). Therefore, the unsubstituted CPA (*R*)-**C2** was also computed as a catalyst to reveal the effect of substituents on the CPA. In the absence of *ortho*-isopropyl groups on the 3,3′-phenyl rings of (*R*)-**C2**, the key step (CPA-induced S$_N$2-type ring opening of the thiolactam to the epoxide) becomes less selective. The calculated energy difference between the two key transition states (**TS5-S** and **TS5-R**) decreases to 1.0 kcal mol^{-1}, indicating significantly lower enantioselectivity for the reaction. The predicted *ee* value decreases to 69%, which shows the same trend as the experimental observation (31%). Notably, the reacting epoxide in **TS5-S** has a favorable conformation, which can be attributed to the absence of the isopropyl groups in CPA leading to a vacancy for the incoming epoxide. Therefore,
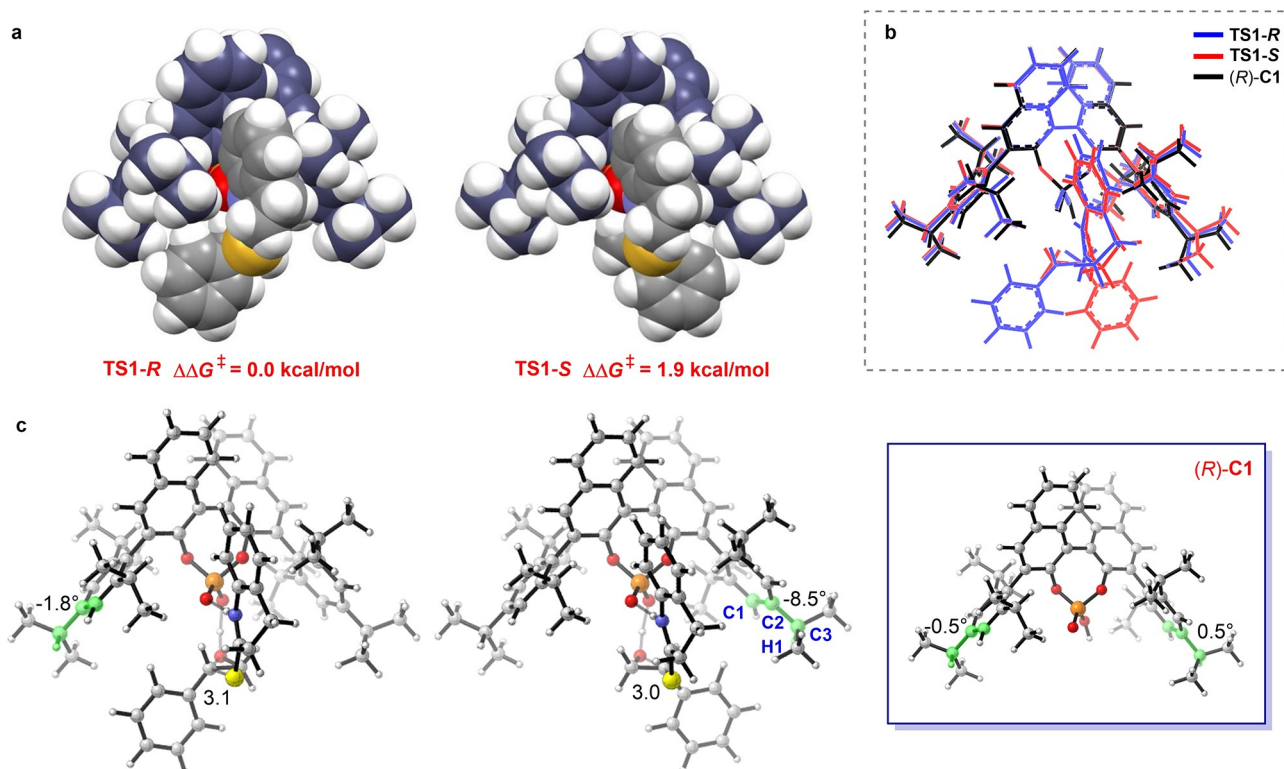

Figure 2. a) Space-filling models of **TS1-R** and **TS1-S**. b) Superimposition of the axial projections of (*R*)-**C1** (black), **TS1-R** (blue), and **TS1-S** (red). c) Axial projections of **TS1-R**, **TS1-S**, and (*R*)-**C1**. The key bond lengths and angles are shown.
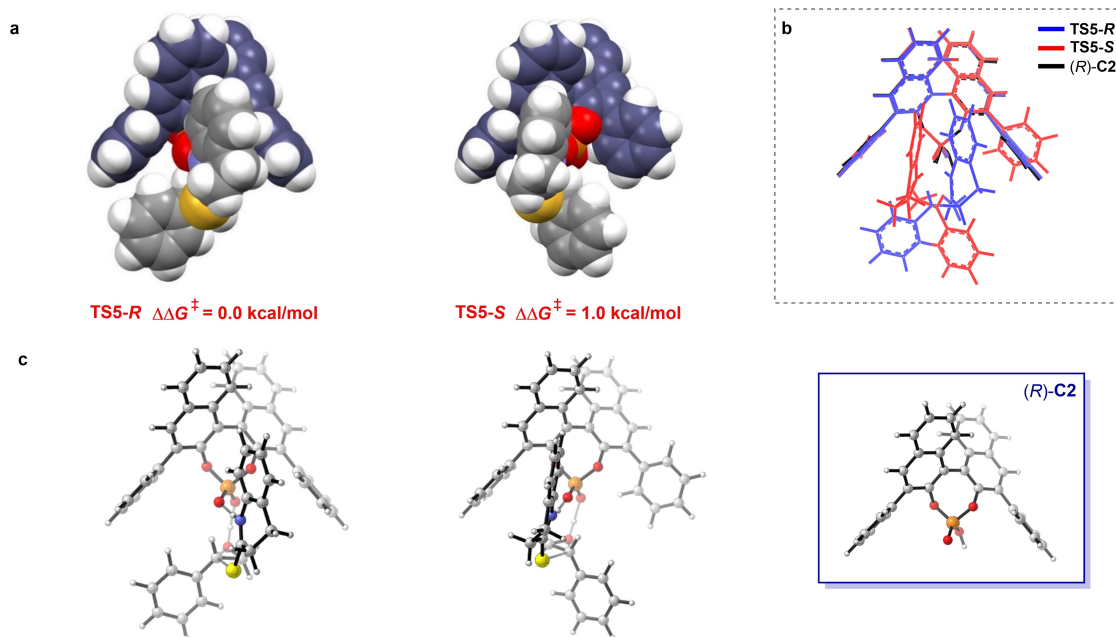
Figure 3. a) Space-filling models of **TS5-R** and **TS5-S**. b) Superimposition of the axial projections of (*R*)-**C2** (black), **TS5-R** (blue), and **TS5-S** (red). c) Axial projections of **TS5-R**, **TS5-S**, and (*R*)-**C2**.

modification of the bulky groups on the phenyl substituent of the CPA causes the change in the enantioselectivity of the epoxide thionation.

Based on our calculations, the enantioselectivity-determining models for the S_N2-type ring opening of the epoxide are summarized in Figure 4. In the first model (Figure 4a),
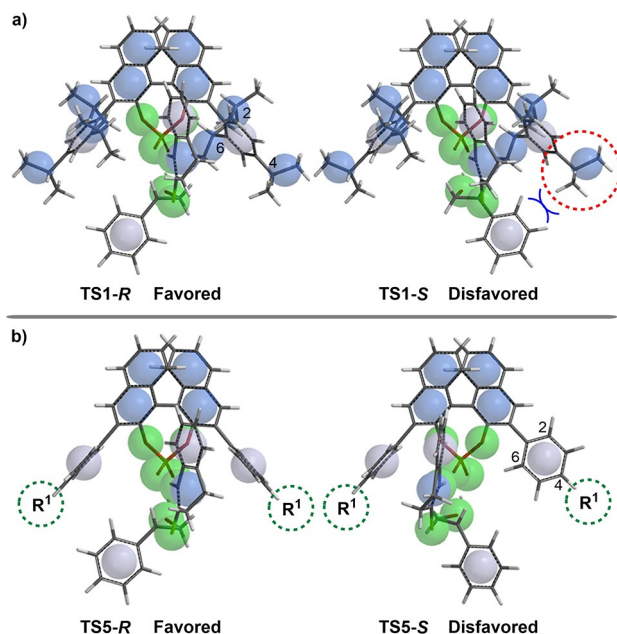

Figure 4. Enantioselectivity-determining models for the key step of S_N2 attack leading to ring opening of the epoxide in the CPA-catalyzed epoxide thionation when the *ortho*-substituents of the 3,3′-phenyl rings are: a) isopropyl groups or b) hydrogen atoms.

the isopropyl groups at the *ortho*-positions fix the orientations of substrates in both possible transition states for activation of the racemic epoxide. As a result, the phenyl ring of the epoxide is much closer to the isopropyl groups of the catalyst in the unfavorable transition state **TS1-S**. Hence, increasing the size of the *para*-substituent groups should enhance the enantioselectivity. In contrast, in the second model (Figure 4b), the absence of *ortho*-isopropyl groups leads to a suitable vacancy for the incoming epoxide in the unfavorable transition state **TS5-S**. The phenyl group of the epoxide is forced to move away to avoid steric repulsion with the *para*-substituents of the CPA. In this case, the presence of bulky *para*-substituent groups on the CPA should not improve the enantioselectivity.

To test these assumptions from the enantioselectivity-determining models, we undertook the computational prediction of the performances of a set of CPA catalysts in epoxide thionation reactions (Figure 5). For CPA (*R*)-**C1**, the first enantioselectivity-determining model is valid because of the presence of *ortho*-isopropyl groups. By contrast, CPAs (*R*)-**C2**, (*R*)-**C3**, and (*R*)-**C4** all contain hydrogen atoms at the *ortho* positions of their 3,3′-phenyl groups and, therefore, they were analysed with the second model shown in Figure 4.

The theoretically predicted and available experimentally observed enantioselectivities for the thionation of epoxides catalyzed by various CPAs are given in Table 1. When R^1 and R^2 are both isopropyl groups ((*R*)-**C1**), the calculated $\Delta\Delta G^{\ddagger}$ value is 1.9 kcal mol^{-1} (entry 1), indicating an *ee* value of 92%. When the R^1 (*para*) and R^2 (*ortho*) groups are changed to hydrogen atoms ((*R*)-**C2**), the calculated $\Delta\Delta G^{\ddagger}$ value decreases to 1.0 kcal mol^{-1} (entry 2). Furthermore, when R^2 is a hydrogen atom and R^1 is either a phenyl or a

a)

b)

(*R*)-**C1**:[a]R[1] = *i*-Pr, R[2] = *i*-Pr
(*R*)-**C2**:[a]R[1] = H, R[2] = H
(*R*)-**C3**:[a]R[1] = Ph, R[2] = H
(*R*)-**C4**:[a]R[1] = *t*-Bu, R[2] = H
(*R*)-**C5**:[a]R[1] = Ph, R[2] = *i*-Pr
(*R*)-**C6**:[a]R[1] = *t*-Bu, R[2] = *i*-Pr
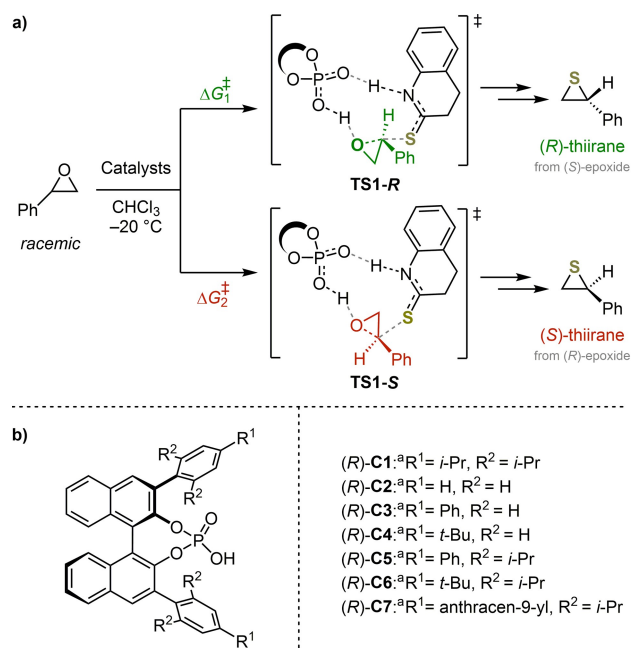(*R*)-**C7**:[a]R[1] = anthracen-9-yl, R[2] = *i*-Pr

Figure 5. a) Transition states considered for the enantioselectivity-determining step of the epoxide thionation. b) Set of CPAs used for the predictive analysis.

tert-butyl group (entries 3 and 4, respectively), the calculated $\Delta\Delta G^{\ddagger}$ values are only 0.7 or 0.4 kcal mol^{-1}. These results agree reasonably well with the experimental observations, thus confirming that the R[2] group is the most influential, and that simply increasing the size of R[1] in the absence of a large R[2] does not improve the enantioselectivity. Other density functionals gave similar predictions, and are described later as well as in the Supporting Information.

Based on the first enantioselectivity-determining model, some new CPA catalysts ((*R*)-**C5**, (*R*)-**C6**, and (*R*)-**C7**) were designed to further improve the enantioselectivity. The key idea is that the *ortho*-isopropyl groups should be maintained. As shown in Table 1 (entry 5), changing R[1] to a phenyl group increases the calculated $\Delta\Delta G^{\ddagger}$ value to 3.1 kcal mol^{-1}. If the size of R[1] is further increased (*tert*-butyl group, entry 6), the corresponding energy difference $\Delta\Delta G^{\ddagger}$ is 3.6 kcal mol^{-1}. Moreover, when R[1] is a 9-anthracenyl ring, the calculated $\Delta\Delta G^{\ddagger}$ value goes up to 4.2 kcal mol^{-1}. These

calculations confirm that increasing the size of the R[1] group leads to higher enantioselectivity in the presence of *ortho*-isopropyl groups. The calculated free energy barriers of the rate-determining step (ΔG_{rds}) with (*R*)-**C5**, (*R*)-**C6**, and (*R*)-**C7** as catalysts are 19.0, 20.4, and 22.9 kcal mol^{-1}, respectively. This suggests that bulky groups at the *para* position should not inhibit reactivity.

Experimental Tests. To test the predicted improvement in enantioselectivity, the thionation of *rac*-styrene oxide (*rac*-**1**) was examined using the chiral phosphoric acids (*R*)-**C5**, (*R*)-**C6**, and (*R*)-**C7** as catalysts under the previously reported conditions,[14] where (*R*)-TRIP ((*R*)-**C1**) performed excellently. The (*R*)-BINOLs required for the synthesis of (*R*)-**C5** and (*R*)-**C6**, containing 2,6-diisopropyl-4-substituted phenyl rings in the 3,3′-positions, were prepared following reported procedures based on Kumada cross-coupling reactions (see the Supporting Information). It is worth mentioning that, for the case when R[1] is 9-anthracenyl (towards (*R*)-**C7**), an approach based on a Negishi cross-coupling led to a more reproducible synthesis, as well as a higher yield of the desired (*R*)-BINOL.

By using (*R*)-**C5** as the catalyst, the reaction of *rac*-**1** with thiolactam **3a** provided thiirane (*R*)-**2** with slightly higher enantioselectivity compared to (*R*)-**C1** (94% *ee*, entry 5). In line with the predictions, when (*R*)-**C6** acted as the catalyst, thiirane (*R*)-**2** was obtained with 96% *ee* (entry 6). Finally, catalyst (*R*)-**C7** also matched the predicted trend, producing (*R*)-**2** with 94% *ee*. This experimental validation further supports that the *ortho*-substituents on CPAs play a significant role in determining the position of the epoxide, and also that increasing the size of the *para*-substituents can lead to higher enantioselectivity. The results obtained with the set of CPAs show a good correlation between the corresponding free energy differences derived from the experiment and from the calculations ($R^2 = 0.85$, Figure 6). We also further evaluated the reactions of several aliphatic epoxides with thiolactam **3a** in the presence of the new CPA catalysts. Unfortunately, both computational and experimental results agreed that the reactions proceed with low enantioselectivity (see Table S2).

To test the accuracy of our computational results on the performance of various catalysts, single-point energies were evaluated with the popular density functionals as well as higher accuracy density functionals: ωB97X-D3, ωB97M-V, ωB97M-D3BJ, ωB97M-D4, and PWPB95-D3BJ using the

Table 1: Theoretically predicted and experimentally observed enantioselectivities for the thionation of *rac*-**1**, catalyzed by various CPAs.

Entry	Catalyst	$\Delta\Delta G^{\ddagger}_{calc}$[a]	$\Delta\Delta G^{\ddagger}_{exp}$[b]	ee_{calc}[c]	ee_{exp}[d]
1	(*R*)-**C1**	1.9	1.9	92	92
2	(*R*)-**C2**	1.0	0.4	69	31
3	(*R*)-**C3**	0.7	0.3	53	24
4	(*R*)-**C4**	0.4	0.1	33	7
5	(*R*)-**C5**	3.1	2.1	99	94
6	(*R*)-**C6**	3.6	2.3	>99	96
7	(*R*)-**C7**	4.2	2.1	>99	94

[a] $\Delta\Delta G^{\ddagger}_{calc} = \Delta G^{\ddagger}_2 - \Delta G^{\ddagger}_1$, where $\Delta G^{\ddagger}_1$ and $\Delta G^{\ddagger}_2$ were obtained by theoretical calculations. [b] $\Delta\Delta G^{\ddagger}_{exp}$ is extrapolated from the experimentally observed *ee* values ($\Delta\Delta G^{\ddagger} = -RT\ln[(1-ee)/(1+ee)]$). [c] *ee* value predicted by theoretical calculations. [d] *ee* values experimentally observed. Energy differences are given in kcal mol^{-1}.
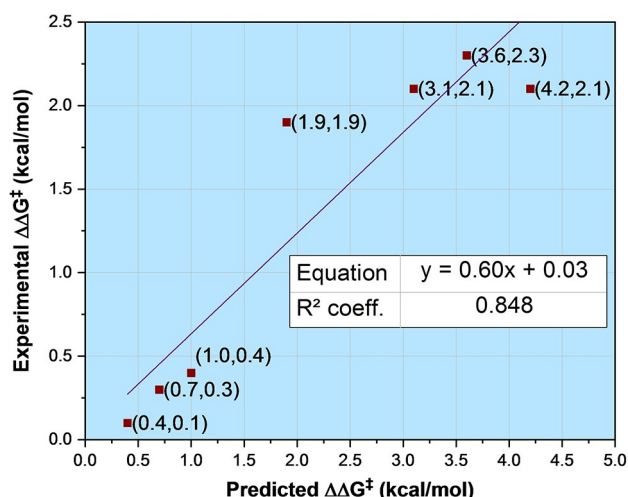
Figure 6. Correlation between the experimental and predicted $\Delta\Delta G^{\ddagger}$ values.

ORCA 5.1.0 program for a comparison of the stereo-selectivities (Table S3).[19] The trends in enantioselectivities are consistent with each of the five DFT methods. For example, with (R)-**C5**, (R)-**C6**, and (R)-**C7**, our standard method predicted energetic preferences for the formation of one stereoisomer of 3.1, 3.6, and 4.2 kcal mol^{-1}, respectively, while the higher accuracy methods gave 2.0–2.5, 3.1–3.4, and 3.6–4.7, respectively. Geometry optimizations were also performed on enantioselectivity-determining steps with the SMD solvation model at the M06-2X/6-31G(d) level of theory to determine the influence of dispersion and solvent effects on geometries. The detailed energy differences are summarized in Table S4; the results are consistent with the methods originally used for the predictions described here.

Conclusion

The mechanism and origin of the enantioselectivity of the CPA-catalyzed epoxide thionation with thiolactam by kinetic resolution have been explored with DFT calculations. The catalytic cycle involves two main steps of nucleophilic ring opening of epoxide and carbonyl elimination. The enantioselectivity-determining step is the first S_N2 ring opening of the epoxide by CPA-activated thiolactam. The observed enantioselectivities result from the steric interaction between the epoxide group and the substituents of the CPA catalyst. Two enantioselectivity-determining models were observed depending on the *ortho*-substituents of the phenyl group attached to the CPAs. The *ortho*-isopropyl groups restrict the position of the epoxide group, leading to alteration of the enantioselectivity as a result of the size of the *para*-substituents. On the basis of this model, some new CPA catalysts were designed and found to improve the enantioselectivity of this reaction.

Conflict of Interest

The authors declare no conflict of interest.

[1] a) T. Akiyama, J. Itoh, K. Fuchibe, *Adv. Synth. Catal.* **2006**, *348*, 999–1010; b) D. Parmar, E. Sugiono, S. Raja, M. Rueping, *Chem. Rev.* **2014**, *114*, 9047–9153; c) D. Parmar, E. Sugiono, S. Raja, M. Rueping, *Chem. Rev.* **2017**, *117*, 10608–10620.

[2] a) M. Rueping, A. Kuenkel, I. Atodiresei, *Chem. Soc. Rev.* **2011**, *40*, 4539–4549; b) M. Terada, *Synthesis* **2010**, 1929–1982.

[3] a) J. S. Lin, T. T. Li, G. Y. Jiao, Q. S. Gu, J. T. Cheng, L. Lv, X. Y. Liu, *Angew. Chem. Int. Ed.* **2019**, *58*, 7092–7096; *Angew. Chem.* **2019**, *131*, 7166–7170; b) J. Yu, F. Shi, L. Z. Gong, *Acc. Chem. Res.* **2011**, *44*, 1156–1171; c) S. L. You, Q. Cai, M. Zeng, *Chem. Soc. Rev.* **2009**, *38*, 2190–2201; d) G. J. Mei, Z. Q. Zhu, J. J. Zhao, C. Y. Bian, J. Chen, R. W. Chen, F. Shi, *Chem. Commun.* **2017**, *53*, 2768–2771; e) Y. Cai, Y. Tang, I. Atodiresei, M. Rueping, *Angew. Chem. Int. Ed.* **2016**, *55*, 14126–14130; *Angew. Chem.* **2016**, *128*, 14332–14336.

[4] a) J. Zhang, P. Yu, S. Y. Li, H. Sun, S. H. Xiang, J. Wang, K. N. Houk, B. Tan, *Science* **2018**, *361*, eaas8707; b) J. P. Reid, L. Simón, J. M. Goodman, *Acc. Chem. Res.* **2016**, *49*, 1029–1041; c) Y. Huang, X. Yang, Z. Lv, C. Cai, C. Kai, Y. Pei, Y. Feng, *Angew. Chem. Int. Ed.* **2015**, *54*, 7299–7302; *Angew. Chem.* **2015**, *127*, 7407–7410; d) S. Li, J. W. Zhang, X. L. Li, D. J. Cheng, B. Tan, *J. Am. Chem. Soc.* **2016**, *138*, 16561–16566.

[5] a) K. Kaupmees, N. Tolstoluzhsky, S. Raja, M. Rueping, I. Leito, *Angew. Chem. Int. Ed.* **2013**, *52*, 11569–11572; *Angew. Chem.* **2013**, *125*, 11783–11786; b) K. Rothermel, M. Melikian, J. Hioe, J. Greindl, J. Gramüller, M. Žabka, N. Sorgenfrei, T. Hausler, F. Morana, R. M. Gschwind, *Chem. Sci.* **2019**, *10*, 10025–10034; c) P. Christ, A. G. Lindsay, S. S. Vormittag, J. M. Neudörfl, A. Berkessel, A. C. O'Donoghue, *Chem. Eur. J.* **2011**, *17*, 8524–8528.

[6] a) I. Ćorić, B. List, *Nature* **2012**, *483*, 315–319; b) L. Xu, H. Chen, J. Liu, L. Zhou, Q. Liu, Y. Lan, J. Xiao, *Org. Chem. Front.* **2019**, *6*, 1162–1167; c) T. Akiyama, *Chem. Rev.* **2007**, *107*, 5744–5758; d) C. Qian, P. Li, J. Sun, *Angew. Chem. Int. Ed.* **2021**, *60*, 5871–5875; *Angew. Chem.* **2021**, *133*, 5935–5939.

[7] a) Y. B. Wang, P. Yu, Z. P. Zhou, J. Zhang, J. J. Wang, S. H. Luo, Q. S. Gu, K. N. Houk, B. Tan, *Nat. Catal.* **2019**, *2*, 504–

513; b) X. Yang, F. D. Toste, *J. Am. Chem. Soc.* **2015**, *137*, 3205–3208; c) J. S. Lin, T. T. Li, J. R. Liu, G. Y. Jiao, Q. S. Gu, J. T. Cheng, Y. L. Guo, X. Hong, X. Y. Liu, *J. Am. Chem. Soc.* **2019**, *141*, 1074–1083; d) H. H. Liao, A. Chatupheeraphat, C. C. Hsiao, I. Atodiresei, M. Rueping, *Angew. Chem. Int. Ed.* **2015**, *54*, 15540–15544; *Angew. Chem.* **2015**, *127*, 15760–15765.

[8] a) M. R. Monaco, B. Poladura, M. Diaz De Los Bernardos, M. Leutzsch, R. Goddard, B. List, *Angew. Chem. Int. Ed.* **2014**, *53*, 7063–7067; *Angew. Chem.* **2014**, *126*, 7183–7187; b) M. Terada, *Chem. Commun.* **2008**, 4097–4112; c) S. Gao, M. Duan, Q. Shao, K. N. Houk, M. Chen, *J. Am. Chem. Soc.* **2020**, *142*, 18355–18368; d) K. Mori, T. Katoh, T. Suzuki, T. Noji, M. Yamanaka, T. Akiyama, *Angew. Chem. Int. Ed.* **2009**, *48*, 9652–9654; *Angew. Chem.* **2009**, *121*, 9832–9834.

[9] a) X. Li, M. Duan, Z. Deng, Q. Shao, M. Chen, G. Zhu, K. N. Houk, J. Sun, *Nat. Catal.* **2020**, *3*, 1010–1019; b) M. Sickert, C. Schneider, *Angew. Chem. Int. Ed.* **2008**, *47*, 3631–3634; *Angew. Chem.* **2008**, *120*, 3687–3690; c) G. Li, J. C. Antilla, *Org. Lett.* **2009**, *11*, 1075–1078.

[10] a) B. Yang, J. Dai, Y. Luo, K. K. Lau, Y. Lan, Z. Shao, Y. Zhao, *J. Am. Chem. Soc.* **2021**, *143*, 4179–4186; b) J. Pous, T. Courant, G. Bernadat, B. I. Iorga, F. Blanchard, G. Masson, *J. Am. Chem. Soc.* **2015**, *137*, 11950–11953; c) A. Suneja, R. A. Unhale, V. K. Singh, *Org. Lett.* **2017**, *19*, 476–479.

[11] a) N. Dong, Z. P. Zhang, X. S. Xue, X. Li, J. P. Cheng, *Angew. Chem. Int. Ed.* **2016**, *55*, 1460–1464; *Angew. Chem.* **2016**, *128*, 1482–1486; b) S. Saha, C. Schneider, *Chem. Eur. J.* **2015**, *21*, 2348–2352; c) D. Huang, X. Li, F. Xu, L. Li, X. Lin, *ACS Catal.* **2013**, *3*, 2244–2247.

[12] a) R. Maji, S. C. Mallojjala, S. E. Wheeler, *Chem. Soc. Rev.* **2018**, *47*, 1142–1158; b) Q. Peng, F. Duarte, R. S. Paton, *Chem. Soc. Rev.* **2016**, *45*, 6093–6107; c) J. P. Reid, J. M. Goodman, *J. Am. Chem. Soc.* **2016**, *138*, 7910–7917; d) P. A. Champagne, K. N. Houk, *J. Am. Chem. Soc.* **2016**, *138*, 12356–12359; e) C. Liu, M. Besora, F. Maseras, *Chem. Asian J.* **2016**, *11*, 411–416.

[13] a) K. Mori, T. Itakura, T. Akiyama, *Angew. Chem. Int. Ed.* **2016**, *55*, 11642–11646; *Angew. Chem.* **2016**, *128*, 11814–11818; b) J. Wang, M. W. Chen, Y. Ji, S. B. Hu, Y. G. Zhou, *J. Am. Chem. Soc.* **2016**, *138*, 10413–10416; c) M. Sakuma, A.

Sakakura, K. Ishihara, *Org. Lett.* **2013**, *15*, 2838–2841; d) D. J. Cheng, L. Yan, S. K. Tian, M. Y. Wu, L. X. Wang, Z. L. Fan, S. C. Zheng, X. Y. Liu, B. Tan, *Angew. Chem. Int. Ed.* **2014**, *53*, 3684–3687; *Angew. Chem.* **2014**, *126*, 3758–3761.

[14] S. Liao, M. Leutzsch, M. R. Monaco, B. List, *J. Am. Chem. Soc.* **2016**, *138*, 5230–5233.

[15] a) P. J. Stephens, F. J. Devlin, C. F. Chabalowski, M. J. Frisch, *J. Phys. Chem.* **1994**, *98*, 11623–11627; b) C. Lee, W. Yang, R. G. Parr, *Phys. Rev. B* **1988**, *37*, 785–789; c) S. S. Meng, P. Yu, Y. Z. Yu, Y. Liang, K. N. Houk, W. H. Zheng, *J. Am. Chem. Soc.* **2020**, *142*, 8506–8513; d) S. Gao, M. Duan, J. Liu, P. Yu, K. N. Houk, M. Chen, *Angew. Chem. Int. Ed.* **2021**, *60*, 24096–24106; *Angew. Chem.* **2021**, *133*, 24298–24308.

[16] a) Y. Zhao, D. G. Truhlar, *Theor. Chem. Acc.* **2008**, *120*, 215–241; b) Y. Zhao, D. G. Truhlar, *Acc. Chem. Res.* **2008**, *41*, 157–167; c) A. V. Marenich, C. J. Cramer, D. G. Truhlar, *J. Phys. Chem. B* **2009**, *113*, 6378–6396.

[17] M. J. Frisch, et al. *Gaussian 09*; Revision D.01, Gaussian, Inc., Wallingford, CT, **2013**. The full author list is shown in the Supporting Information.

[18] a) F. Liu, Y. Liang, K. N. Houk, *Acc. Chem. Res.* **2017**, *50*, 2297–2308; b) F. M. Bickelhaupt, K. N. Houk, *Angew. Chem. Int. Ed.* **2017**, *56*, 10070–10086; *Angew. Chem.* **2017**, *129*, 10204–10221; c) S. Liu, Y. Lei, X. Qi, Y. Lan, *J. Phys. Chem. A* **2014**, *118*, 2638–2645.

[19] a) F. Neese, *Wiley Interdiscip. Rev.: Comput. Mol. Sci.* **2012**, *2*, 73–78; b) Y. S. Lin, G. D. Li, S. P. Mao, J. D. Chai, *J. Chem. Theory Comput.* **2013**, *9*, 263–272; c) N. Mardirossian, M. Head-Gordon, *J. Chem. Phys.* **2016**, *144*, 214110; d) A. Najibi, L. Goerigk, *J. Chem. Theory Comput.* **2018**, *14*, 5725–5738; e) A. Najibi, L. Goerigk, *J. Comput. Chem.* **2020**, *41*, 2562–2572; f) L. Goerigk, S. Grimme, *J. Chem. Theory Comput.* **2011**, *7*, 291–309.